HHS Public Access

Author manuscript

Nat Neurosci. Author manuscript; available in PMC 2016 September 28.

Published in final edited form as:

Nat Neurosci. 2016 May ; 19(5): 725–733. doi:10.1038/nn.4281.

VTA glutamatergic inputs to nucleus accumbens drive aversion by acting on GABAergic interneurons

Jia Qi, **Shiliang Zhang**, **Hui-Ling Wang**, **David J. Barker**, **Jorge Miranda-Barrientos**, and **Marisela Morales***

Neuronal Networks Section, Integrative Neuroscience Research Branch, National Institute on Drug Abuse, 251 Bayview Blvd Suite 200, Baltimore, MD 21224, United States

Abstract

The ventral tegmental area (VTA) is best known for its dopamine neurons, some of which project to nucleus accumbens (nAcc). However, the VTA also has glutamatergic neurons that project to nAcc. The function of the mesoaccumbens-glutamatergic pathway remains unknown. Here, we report that nAcc photoactivation of mesoaccumbens-glutamatergic fibers promotes aversion. Although we found that these mesoaccumbens-glutamate-fibers lack GABA, the aversion evoked by their photoactivation depends on glutamate and GABA receptor signaling, and not on dopamine receptor signaling. We found that mesoaccumbens-glutamatergic-fibers establish multiple asymmetric synapses on single parvalbumin-GABAergic interneurons, and that nAcc photoactivation of these fibers drives AMPA-mediated cellular firing of parvalbumin-GABAergic interneurons. These parvalbumin-GABAergic-interneurons, in turn, inhibit nAcc medium spiny output neurons, as such, controlling inhibitory neurotransmission within nAcc. The mesoaccumbens-glutamatergic pathway is the first glutamatergic input to nAcc shown to mediate aversion, instead of reward, and the first pathway shown to establish excitatory synapses on nAcc parvalbumin-GABAergic interneurons.

Keywords

VTA; nucleus accumbens; parvalbumin interneurons; VGluT2; aversion; TH

***Correspondence**: Marisela Morales. National Institutes of Health. National Institute on Drug Abuse. Intramural Research Program. Neuronal Networks Section. 251 Bayview Boulevard, Baltimore, MD 21224. ; Email: mmorales@intra.nida.nih.gov

Conflict of Interest: The authors declare that they do not have any conflicts of interest (financial or otherwise) related to the data presented in this manuscript.

Author Contributions. M.M. conceptualized the project. J.Q. performed behavioral and pharmacological studies. J.Q. and D.B. analyzed the behavioral experiment data. J.Q., S.Z. and H.W. performed neuroanatomy and immunolabeling studies. H.W. performed *in situ* hybridization. J.Q. and S.Z. performed confocal microscopy studies. S.Z. performed electron microscopy studies. J.M. performed electrophysiological studies. All authors participated in the conception and experimental design, and data interpretation. M.M. wrote the manuscript with the participation of all authors.

Competing Financial Interests. The authors declare no competing financial interests.

INTRODUCTION

The nucleus accumbens (nAcc) is a heterogeneous brain structure that has been implicated in both reward and aversion [1, 2]. The nAcc receives dopamine (DA) afferents from the ventral tegmental area (VTA) and glutamate afferents from the medial prefrontal cortex, basolateral amygdala, ventral hippocampus, subiculum, and paraventricular nucleus of the thalamus [3-7]. The DA inputs establish symmetric synapses on nAcc medium spiny neurons (MSNs), and are thought to integrate dopaminergic reinforcing signals [8, 9]. In contrast, the glutamatergic afferents establish asymmetric synapses on the same MSNs [10], and are thought to convey different types of reward-related information during goal-directed behavior [11]. Recent optogenetic studies have shown that activation of glutamatergic inputs from the basolateral amygdala or the ventral hippocampus to nAcc shell facilitates reward seeking [3, 12].

In addition to DA-neurons, the VTA has GABAergic and glutamatergic neurons that also innervate the nAcc [13-18]. The VTA-DA neurons targeting nAcc have been proposed to signal both rewarding and aversive events [19, 20]. Recent studies have shown that the VTA-GABAergic neurons targeting nAcc participate in reward consumption [17] and associative learning [21]. However, the function of VTA-glutamatergic neurons targeting the nAcc remains to be determined.

The VTA-glutamatergic neurons selectively express the vesicular glutamate transporter 2 (VGluT2) [18, 22]. A subset of them coexpresses tyrosine hydroxylase, TH (VGluT2-TH neurons) [23], and innervates nAcc [24]. When VGluT2-TH fibers from VTA are photoactivated in nAcc, excitatory postsynaptic currents (EPSCs) are recorded in nAcc MSNs and interneurons [14, 15, 25], and release of DA and glutamate is evoked from different axonal compartments within the same axon [26].

Here, we found that VTA-VGluT2 fibers heavily innervate nAcc medial (m) Shell (mesoaccumbens glutamatergic inputs) where they establish only asymmetric synapses, and that their photoactivation promotes conditioned place aversion, which depends on glutamate and GABA receptors. Within nAcc mShell, the VTA-VGluT2 fibers establish multiple asymmetric synapses on single parvalbumin (PV) GABAergic interneurons. Moreover, photoactivation of nAcc mShell VTA-VGluT2 fibers induces *in vivo* expression of c-Fos in PV-interneurons, and *ex vivo* cellular firing of PV-GABAergic interneurons. Aversion is also elicited by direct photoactivation of nAcc PV interneurons (expressing channelrhodopsin-2, ChR2, under the regulation of the *pv*-promoter). Thus we reveal an unanticipated role of VTA-glutamatergic inputs to nAcc in promoting aversion, rather than reward, by regulating the firing of PV-GABAergic interneurons.

RESULTS

VGluT2-mesoaccumbens fibers synapsing in the nAcc

We first targeted VTA-glutamatergic neurons and their axons by injecting a cre-inducible adeno-associated virus (AAV) with double-floxed inverted open reading frame (DIO) expressing ChR2 fused with enhanced yellow fluorescent protein (eYFP; VGluT2-ChR2-

eYFP mice) or mCherry into VTA of VGluT2::Cre transgenic mice (**Fig. 1a**). We have previously shown the VTA-selective expression of Cre-inducible reporter genes under the *vglut2*-promoter in neurons expressing *vglut2* mRNA [27]. Here, we targeted viral injections into VTA (**Fig. 1b**), but because numerous VGluT2-neurons surround the mouse VTA [18, 28], we first verified that infected neurons were confined to the VTA by analyzing the rostro-caudal expression of eYFP or mCherry (**Supplementary Fig. 1**). Within nAcc, we found that the fibers expressing eYFP or mCherry under the regulation of the *vglut2*-promoter were predominantly localized in the mShell (**Fig. 1c,d**), and sometimes extended into the ventromedial Shell and olfactory tubercle (**Fig. 1c** and **Supplementary Fig. 2a**).

We next analyzed the characteristics of VTA-VGluT2 inputs within nAcc-mShell by immunoelectron microscopy. We detected mCherry (from infected VTA-VGluT2 neurons) confined to axons and axon terminals. The mCherry axon terminals established asymmetric (excitatory-type) synapses on dendrites (**Fig. 1e**). These mCherry axon terminals were found to coexpress VGluT2-immunolabeling (**Fig. 1e**), thus indicating that the VGluT2-fibers from the VTA establish excitatory-type synapses within nAcc mShell.

Behaviors promoted by VGluT2-mesoaccumbens-fibers

To assess the behavioral consequence of activation of VTA-VGluT2-fibers innervating nAcc-mShell (mesoaccumbens-glutamatergic inputs), we implanted optical probes bilaterally in nAccmShell to photostimulate VGluT2-mesoaccumbens-fibers in behaving mice (**Fig. 2** and **Supplementary Fig. 2**). VGluT2-ChR2-eYFP and VGluT2-eYFP (control) mice were tested in a three-chamber apparatus and given continuous trains of photostimulation whenever they entered and for as long as they remained in one of the chambers (photostimulation-paired chamber). VGluT2-eYFP mice spent similar times in the two chambers, whereas VGluT2-ChR2-eYFP mice spent significantly less time in the photostimulation-paired chamber (**Fig. 2c**). After two days of testing under conditions where the VGluT2-ChR2-eYFP mice controlled the stimulation, the mice were tested in the absence of stimulation; on this day the mice avoided the chamber where they had previously received the photostimulation (**Fig. 2c** and **Supplementary Fig. 2c**). Thus, VGluT2-ChR2-eYFP mice avoided the photostimulation and acquired a conditioned aversion to the stimulation-paired chamber as reflected by their avoidance of this chamber during the stimulation-free test day. However, the conditioned aversion observed 24 hours after last photostimulation (Test 1; **Supplementary Fig. 2e**) was no longer observed after additional 24 hours (Test 2; **Supplementary Fig. 2e**).

We further determined whether the photostimulation of VGluT2-mesoaccumbens-fibers would establish escape-avoidance responding in a negative-reinforcement task. Mice were placed in an apparatus featuring two wheels for operant responding, and were required to turn the right wheel (Days 1-6) or left wheel (Reversal Days 1-4) in order to terminate (for 2 s) ongoing photostimulation (20 Hz, 0.5 s on/off) (**Fig. 2d)**. VGluT2-ChR2-eYFP mice rotated the “active wheel” (which resulted in photostimulation time out) significantly more than the “inactive wheel” (**Fig. 2e**), and significantly more than the VGluT2-eYFP during both initial training and reversal training (**Fig. 2e**). Thus VGluT2-ChR2-eYFP mice

discriminate the photostimulation as an aversive stimulus, and learned to avoid this aversive stimulation by rotating the wheel.

We next tested whether photoactivation of VGluT2-mesoaccumbens-fibers would disrupt positive reinforcement for a natural reward. In a two-lever chamber, mice were first trained to press either lever to earn food pellets. Following stable responses (Days 1 to 3), lever presses on one of the two food-delivering levers resulted in nAcc-mShell photostimulation of VGluT2-mesoaccumbens-fibers along with a food pellet (1 s, 20 Hz; **Fig. 2f**). As a result of photostimulation, VGluT2-ChR2-eYFP mice made significantly fewer lever presses for the photostimulation-paired lever than the unpaired lever (**Fig. 2g**). To gain the food pellets, the VGluT2-ChR2-eYFP mice made more lever presses for the stimulation-unpaired lever (right lever on days 4 and 5, left lever on days 7 and 8). The VGluT2-ChR2-eYFP mice quickly learned not to press the lever associated with photostimulation.

To determine the conditioned response to the photoinhibition of VGluT2-mesoaccumbens-fibers, the viral vector AAV-DIO expressing halorhodopsin (eNpHR) fused with eYFP was delivered into VTA of VGluT2::Cre mice (VGluT2-eNpHR-eYFP mice). The VGluT2-eNpHR-eYFP and control (VGluT2-eYFP) mice were tested under the place conditioning paradigm (**Fig. 3a, b**), and found that neither VGluT2-eNpHR-eYFP mice nor VGluT2-eYFP mice showed preference or aversion to the photoinhibition-associated chamber (**Fig. 3c**). To test whether photoinhibition of VGluT2-mesoaccumbens-fibers was able to affect the aversion from unpredictable foot-shock, which is known to induce learned helplessness, we evaluated the immobility score of the forced swim test before and after sessions of inescapable foot shock delivery (**Fig. 3d**). While the VGluT2-eYFP mice showed increased immobility in the forced swim test, photoinhibition of VGluT2-mesoaccumbens-fibers in VGluT2-eNpHR-eYFP mice prevented increased immobility in the forced swim test (**Fig. 3e**).

Receptors participating in VGluT2-mesoaccumbens aversion

Given that some VTA-VGluT2 neurons corelease glutamate and DA [26] while others corelease glutamate and GABA [29], we next evaluated the effects of intra-nAcc injections of glutamate, GABA or DA receptor antagonists on the aversion driven by photoactivation of VGluT2-mesoaccumbens-fibers (**Fig. 4**). Ten minutes prior to testing in the three-chamber apparatus, different groups of mice received intra-nAcc injections of a mix of NMDA (MK801)/AMPA (CNQX) receptor antagonists, a mix of GABAa (bicuculline)/GABAb (saclofen) receptor antagonists, dopamine D1 receptor antagonist (SCH23390), a D2 receptor antagonist (eticlopride) or a mix of SCH23390 and eticlopride (**Fig. 4b**). Control mice that received only artificial cerebrospinal fluid (ACSF), avoided the photostimulation-paired chamber on the conditioning day (**Fig. 4c**). In contrast, mice that received MK801/CNQX or bicuculline/saclofen did not avoid the chamber where they received photostimulation of VGluT2-mesoaccumbens-fibers (**Fig. 4c** and **Supplementary Fig. 3**). Intra-nAcc administration of SCH23390, eticlopride, or a mix of SCH23390 and eticlopride did not block the aversion produced by photostimulation of the VGluT2-mesoaccumbens-fibers (**Fig. 4c**). Thus the aversive effects of activation of the mesoaccumbens-glutamatergic pathway were mediated by nAcc signaling of both glutamate and GABA receptors.

We next applied a combination of anatomical approaches to explore the possible mechanism by which signaling of glutamate and GABA receptors may participate in the aversion induced by activation of the mesoaccumbens-glutamatergic-pathway. Knowing that most VTA-VGluT2 neurons projecting to lateral habenula coexpress glutamate acid decarboxylases (*gad65/67*, GADs; responsible for the synthesis of GABA), and corelease glutamate and GABA from the same axon terminal [29], we determined whether any such neurons project to nAcc-mShell. By a combination of FluoroGold (FG) retrograde tract tracing, immunohistochemistry and dual *in situ* hybridization, we found that most VTAVGluT2 neurons projecting to nAcc-mShell lacked *gad65/67* mRNA (90%; 172 out of 192 VGluT2 neurons; **Fig. 5** and **Supplementary Fig. 4**). The lack of coexpression of *gad65/67* mRNA in the majority of VGluT2-mesoaccumbens neurons suggests that these neurons do not have the capability to synthesize GABA, and that they may not corelease glutamate and GABA in nAcc-mShell. However, recent electrophysiological studies suggest that DA-axon terminals may release GABA in the striatum, even in the absence of *gad65/67* [30]. Because we found that more than half of the VGluT2-mesoaccumbens neurons coexpressed TH (VGluT2-TH neurons; 64%; 122 out of 192; **Fig. 5** and **Supplementary Fig. 4**), we determined the extent to which these glutamatergic-dopaminergic (VGluT2-TH) mesoaccumbens neurons contribute to aversion. We compared conditioned place aversion between animals that received intra-nAcc injections of vehicle or dopaminergic neurotoxin 6-hydroxydopamine (6-OHDA). We confirmed degeneration of DA-axons by *post hoc* brain analysis after behavioral testing. Animals treated with 6-OHDA resulted in the loss of TH-immunoreactivity within the nAcc-mShell without affecting aversion induced by activation of the mesoaccumbens-glutamatergic-pathway (**Supplementary Fig. 5**). These results suggest a lack of a major participation of VTA dual VGluT2-TH neurons in mediating aversion induced by photoactivation of VGluT2-mesoaccumbens-fibers.

To directly test the possible involvement of mesoaccumbens-GABA-neurons in place aversion, ChR2-eYFP was induced in VTA-neurons under the regulation of the vesicular GABA transporter promoter (*vgat*-promoter) (VGAT-ChR2-eYFP mice; **Supplementary Fig. 6a,b**). In contrast to the high expression of VGluT2-mesoaccumbens-fibers observed in nAcc-mShell (**Fig. 1c** and **Supplementary Fig. 2a**), the VGAT-mesoaccumbens-fibers were sparse in both shell and core of nAcc (**Supplementary Fig. 6c-e**), as recently reported [31]. Photoactivation of these VGAT-mesoaccumbens-fibers did not induce place aversion, place preference (**Supplementary Fig. 6f,g**) or change in locomotion (**Supplementary Fig. 6h**). Thus findings from these studies together with those obtained from 6-OHDA lesions suggest that GABA release from mesoaccumbens-fibers does not mediate the signaling of GABA receptors within nAcc.

VGluT2-mesoaccumbens-fibers activate PV interneurons

Considering that the VGluT2-mesoaccumbens-fibers do not seem to corelease glutamate and GABA, we hypothesized that VGluT2-mesoaccumbens-fibers synapsing on nAcc GABAergicinterneurons induce release of GABA, accounting for activation of nAcc GABA-receptors, evoked by nAcc photostimulation of VGluT2-mesoaccumbens-fibers. To test this hypothesis, we determined whether photoactivation of VGluT2-mesoaccumbens-fibers induced c-Fos (marker of neuronal activation) in nAcc GABAergic-interneurons (PV- or

nitric oxide synthase; NOS-interneurons) [32, 33], and found that nAcc photoactivation of VGluT2-mesoaccumbens-fibers induced c-Fos expression in local PV-GABAergic interneurons, but not in NOS-GABAergic-interneurons or cholinergicinterneurons (**Supplementary Fig. 7**, and **Supplementary Table 1**). In contrast to c-Fos induction in PV-GABAergic-interneurons in nAcc of VGluT2-ChR2-eYFP mice, the number of MSNs coexpressing c-Fos was lower in these mice than in the controls (VGluT2-eYFP mice; **Supplementary Table 2**), suggesting that activation of PVGABAergic-interneurons affects c-Fos expression in MSNs. Because c-Fos induction was preferentially observed in PV-GABAergic-interneurons, we next determined whether or not VGluT2-mesoaccumbens-fibers synapse on PV-GABAergic-interneurons.

By confocal microscopy we detected mCherry-VGluT2 immunofluorescence varicosities in the nAcc-mShell. After 3-dimensional reconstruction of dual mCherry-VGluT2 immunofluorescence varicosities, we determined that they made contacts along the proximal and distal aspects of a single PV-dendrite (**Fig. 6a-c**) or around the PV-cell body (**Fig. 6h**). We analyzed the distribution of 447 of these dual mCherry-VGluT2 immunofluorescence varicosities contacting PV-interneurons, and found that most of these varicosities (81.56 ± 1.03%) made contacts on PV-dendrites, and fewer (18.44 ± 1.03%) on PV-cell bodies (t_3 = 30.72, P <0.01). By immunoelectron microscopy and serial sectioning, we confirmed that dual mCherry-VGluT2 varicosities correspond to axon-terminals. These mCherry-VGluT2 axon-terminals formed multiple asymmetric (excitatory-type) synapses with a single PV-dendrite (**Fig. 6d-g**) or with a single PV-cell body (**Fig. 6i-k**). We analyzed 138 of these mCherry-VGluT2 terminals making asymmetric synapses on PV-interneurons, and found that most of them (79.98 ± 6.50%) synapsed on PV-dendrites and fewer (20.02 ± 6.50%) on PV-cell bodies (t_3 = 4.613, P = 0.0192). In a separate study, we found that synapses between VGluT2-terminals and PV-interneurons were maintained after nAcc 6-OHDA lesion (**Supplementary Fig. 5de**), suggesting a major input to PV from VGluT2-only neurons. The detection of multiple terminals from VGluT2-mesoaccumbens-fibers containing VGluT2 and making asymmetric synapses on individual PV-neurons suggest that VGluT2-mesoaccumbens-fibers provide a strong monosynaptic excitatory regulation on PV-GABAergic interneurons. Based on these anatomical observations, we hypothesized that nAcc activation of mesoaccumbens-fibers evoke firing of PV-interneurons. To test this hypothesis, we recorded nAcc PV-interneurons in response to optical activation of mesoaccumbens-fibers (**Fig. 7**).

Because the number of nAcc PV-interneurons is very small, cellular recordings were done in nAcc slices from PV-interneurons expressing eYFP under the regulation of the *pv*-promoter (**Fig. 7a-c**). Photoactivation of mesoaccumbens fibers evoked EPSCs in PV-fluorescent neurons (**Fig. 7a-c**), which were characterized as fast spiking interneurons (**Fig. 7d**, and **Supplementary Fig. 8**). A single pulse of photoactivation of mesoaccumbens-fibers elicited potential firing in nAcc PV-interneurons (**Fig. 7e**), which amplitude was not significantly affected by bicuculline (GABAa receptor antagonist), but was blocked by CNQX (AMPA/kainate receptor antagonist; **Fig. 7f**). Given that photoactivation of mesoaccumbens-fibers elicited the firing of PV-interneurons, and because it is well established that PV-interneurons provide a feedforward inhibition to MSNs, we determined whether photoactivation of

mesoaccumbens-fibers induces polysynaptic GABA release onto MSNs. To discriminate direct excitatory inputs from mesoaccumbens-fibers and indirect local inhibitory inputs onto MSNs, nAcc-shell MSNs were recorded at a holding potential of −70 mV or −45 mV (**Supplementary Fig. 9**). Photoactivation of mesoaccumbens-fibers evoked inward currents (EPSCs) in MSNs when recorded at −70 mV (**Supplementary Fig. 9b**), and fast inward currents followed by delayed outward currents (IPSCs) when recorded at −5mV (**Supplementary Fig. 9c**). Bath application of bicuculline blocked the IPSCs without affecting the EPSCs (**Supplementary Fig. 9c**). In contrast, CNQX application alone or in combination with bicuculline blocked both EPSCs and IPSCs, indicating that the IPSCs depended on the activation of glutamate receptors (**Supplementary Fig. 9c-d**), and suggesting that photoactivation of mesoaccumbens-fibers evokes polysynaptic release of GABA from PV-interneurons onto MSNs (**Supplementary Fig. 9e**).

Activation of nAcc PV-interneurons promotes place aversion

To directly examine the participation of nAcc PV-GABAergic interneurons in aversion, the viral vector AAVDIO-ChR2-eYFP was delivered into the nAcc of PV::Cre mice (PV-ChR2-eYFP mice). The PV-ChR2-eYFP and control (PV-eYFP) mice were tested under the place conditioning paradigm (PV-ChR2-eYFP mice; **Supplementary Fig. 10**). While photostimulation of nAcc had no effects on place preference in control mice (PV-eYFP mice), the PV-ChR2-eYFP mice not only avoided the place where the stimulation was given, when the stimulation was available, but they also avoided the chamber where they had previously received the photostimulation (**Supplementary Fig. 10f**), when no stimulation was given. Thus, PV-ChR2-eYFP mice avoided the photostimulation and acquired a conditioned aversion to the stimulation-paired chamber.

DISCUSSION

The nAcc consists of a major population of projection MSNs (95% of nAcc neurons), and a smaller population of GABAergic- and cholinergic-interneurons from which PV-GABAergic-interneurons constitute around 3% [33]. Here we provide converging evidence showing that PV-GABAergic-interneurons are activated in nAcc-shell by glutamatergic-inputs from VTA neurons. We found that activation of these glutamatergicmesoaccumbens-inputs evokes conditioned aversion in mice, which is mediated by activation of both glutamate- and GABA-receptors, but independent of the activation of DA-receptors. Because we found that the vast majority of glutamatergicmesoaccumbens-neurons lack GABAergic markers, we propose that VTA-glutamatergic-inputs drive aversion by a mechanism in which MSNs activity is inhibited by the release of GABA from PV-interneurons, which are excited by VTA-glutamatergic-inputs. We provide evidence that activation of VTA-glutamatergic-inputs to the nAcc is aversive, rather than rewarding.

VTA-VGluT2-only neurons control nAcc PV- interneurons

Converging evidence has shown that while all VTA-glutamatergic-neurons selectively express *vglut2* mRNA, they are diverse in their biochemical composition and connectivity [18, 27, 29, 34]. The diversity among VTA-VGluT2-neurons has led to the suggestion that these neurons participate in a multiplexed neurochemical signaling [35]. A

major class of VTA-VGluT2-neurons lacks both TH- and GABAergic-markers (VGluT2-only-neurons) [18]. A minor class of VTA-VGluT2-neurons coexpresses TH (VGluT2-TH-neurons) from which some of them coexpresses molecules necessary for DA-synthesis and DA-vesicular transport [34]. Another minor class of VTA-VGluT2-neurons coexpresses GABAergic markers from which a single axon terminal coreleases glutamate and GABA, and constitute the major mesohabenular input to lateral habenula glutamatergic-neurons [29]. We found here that the VGluT2-GABAergic-neurons rarely innervate nAcc-mShell, and that VGluT2-neurons (more than half of them coexpressing TH) constitute near to one quarter of the mesoaccumbens-neurons targeting nAcc-mShell. Thus there is the possibility that excitatory inputs from both VTA-VGluT2-only-neurons and VTA-VGluT2-TH-neurons may contribute to the aversion mediated by excitation of glutamatergicmesoaccumbens-fibers synapsing on nAcc PV-GABAergic-interneurons. However, we found that nAcc degeneration of DA-axons does not eliminate glutamatergicmesoaccumbens-fibers synapsing on PV-GABAergic-interneurons. Moreover, nAcc degeneration of DA-axons does not eliminate conditioned aversion induced by activation of glutamatergic-mesoaccumbens-fibers. Thus we propose that the glutamatergic-mesoaccumbens-fibers synapsing on nAcc PV-GABAergic-interneurons are mostly from VTA-VGluT2-only neurons, rather than from VTA-VGluT2-TH-neurons.

The glutamatergic-mesoaccumbens-pathway shown here to form asymmetric synapses on PV-GABAergic-interneurons is the first anatomically identified glutamatergic-pathway to GABAergic-interneurons within the nAcc. In contrast, it is well established that cortical-glutamatergic-inputs from motor and somatosensory cortices synapse on dorsal striatum PV-GABAergic-interneurons, and regulate the activity of these interneurons [35, 36]. Based on ultrastructural and electrophysiological findings reported here, we propose that VTA-VGluT2-neurons provide a major glutamatergic control on nAcc PV-GABAergic-interneurons. At the ultrastructural levels, we revealed that a single dendrite from a PV-GABAergic-interneuron establishes asymmetric synapses with multiple glutamatergic-mesoaccumbens-terminals, which contain VGluT2-protein for the vesicular accumulation and release of glutamate. In addition to dendrites, the cell bodies of nAcc PV-GABAergic-interneurons establish asymmetric synapses with glutamatergic-mesoaccumbens-terminals. These findings indicate that the glutamatergic-mesoaccumbens-pathway provides to a single nAcc PV-GABAergicinterneuron multiple synaptic sites for glutamate release along its dendrites and cell body. In addition, we demonstrated that nAcc photoactivation of mesoaccumbens-inputs drives glutamate receptor mediated firing of nAcc PV-GABAergic-interneurons, and the *in vivo* expression of c-Fos in nAcc PV-GABAergic-interneurons. Importantly, prior studies have established that the synaptic potential generated from a single PVGABAergic-interneuron is able to delay or block the generation of action potentials in a large number of postsynaptic MSNs [37]. This powerful regulation is due to the multiple synapses that a single PV-interneuron establishes with MSNs [38–40], and by the electrotonic synapses among PV-interneurons [38]. GABAergic-interneurons provide feedforward inhibition that regulates spike timing in MSNs, thereby regulating striatal output. Here, we show that activation of glutamatergic inputs from the VTA innervating nAcc PV-GABAergic-interneurons releases GABA onto MSNs, and induces aversion. The demonstration that glutamatergic-mesoaccumbens-fibers synapsing on PV-interneurons

drive aversion is the first evidence suggesting a role for nAcc GABAergicinterneurons in aversion. Although there are collaterals between nAcc MSNs neurons, the major inhibitory control on MSNs is from the PV-GABAergic-interneurons [37, 38, 41], neurons that are the predominant target of the VTA-nAcc glutamate projection.

VGluT2-TH-neurons control MSNs and cholinergic-interneurons

Recent neurochemical and ultrastructural studies have revealed that VGluT2-TH-mesoaccumbens fibers release DA and glutamate from different pools of vesicles [26]. Within these dual VGluT2-TH-axons, the VGluT2-vesicles are concentrated in axon-terminals that form asymmetric synapses on dendritic spines of MSNs [26]. Although a small number of VGluT2-TH neurons innervate the nAcc [18], nAcc activation of fibers from these VGluT2-TH neurons reportedly evokes small EPSCs in each tested nAcc MSN, without resulting in the firing of these neurons [14, 15]. These electrophysiological findings suggest that VGluT2-TH axon-terminals establish infrequent synapses on individual MSNs. While nAcc photoactivation of mesoaccumbens-fibers expressing ChR2 under the *vglut2*-promoter likely resulted in activation mesoaccumbens-fibers from both VTA-VGluT2-only and VTA-VGluT2-TH neurons, this activation did not elicit reward. The lack of elicited reward by activation of glutamatergic-mesoaccumbens-inputs may be explained, in part, by the fact that this activation alone does not result in the firing of MSNs [42]. However, it is also conceivable that GABA release from concomitant mesoaccumbens activation on PV-interneurons may diminish the glutamatergic-mesoaccumbens effects on MSNs (shown in the present study), resulting in induction of a general inhibition on MSNs outputs and the mediation of aversion.

In vitro electrophysiological studies have shown that, in addition to MSNs, nAcc activation of VGluT2-TH fibers evokes EPSCs on cholinergic-interneurons in nAccmShell [25]. However, by *in vivo* optical stimulation we did not detect c-Fos induction in nAcc-cholinergic-interneurons. It is unclear whether the lack of c-Fos induction was due to neuronal network conditions or due to the post-burst hyperpolarization (mediated by SK channels and increased by DA and muscarinic receptors) that cholinergicinterneurons experience after activation of VGluT2-TH-fibers [25]. The activation of DA-receptors, that augments post-burst hyperpolarization, may be mediated by DA corelease with glutamate from glutamate-DA fibers or by DA release known to be evoked by the firing of cholinergic interneurons [43, 44]. While we cannot discard the possibility that the lack of c-Fos detection in cholinergic-interneurons was due to the *in vivo* optical-evoked GABA release from PV-GABAergic interneurons, this seems unlikely, as striatal PV-GABAergic-interneurons do not seem to establish synaptic contacts with cholinergic-interneurons [45].

A role for nAcc PV-GABAergic-interneurons in aversion

While it is well established that nAcc PV-interneurons play a crucial role in the regulation of nAcc neuronal activity, there has been, until now, a lack of information on the inputs that regulate the activity of these interneurons and their possible roles in behavior. Here, we demonstrate that aversion is elicited by direct photoactivation of nAcc PV-interneurons (expressing ChR2, under the regulation of the *pv*-promoter). We showed that these

interneurons are a major target of VTA-glutamatergic-efferents, and that the activation of these efferents synapsing on PV-GABAergic-interneurons releases GABA onto MSNs.

Accumulating evidence has shown biochemical heterogeneity among VTA-glutamatergic neurons [13], leading to the suggestion that VTA-glutamatergic neurons participate in a multiplexed neurochemical signaling by releasing different neurotransmitters [46]. Although, it is unclear the extent to which the different identified types of VTA-glutamatergic neurons participate in diverse behaviors, emerging evidence shows that subsets of VTA-glutamatergic neurons participate in either aversion or reward. While aversion is driven by activation of VTA-glutamatergic-fibers in either lateral habenula [27] or nAcc (present study), reward is driven by activation of VTA-glutamatergic neurons [47]. The aversion driven by mesohabenbular-glutamatergic-fibers in lateral habenula involves activation of glutamate receptors located in glutamatergic-neurons [29], while the aversion driven by mesoaccumbens-glutamatergic-fibers in nAcc involves activation of glutamate receptors located in PV-GABAergic-interneurons. In contrast, the reward driven by activation of glutamatergic-neurons within VTA involves activation of glutamate receptors located in neighboring DA neurons that innervate the nAcc [47]. Thus it seems that the participation of VTA-glutamatergic neurons in aversion or reward may depend not only on the phenotype of these neurons, but may also depend on the cellular phenotype of their postsynaptic targets.

Online Methods

Methods and any associated references are available in the online version of the paper.

All animal procedures were performed in accordance with NIH Guidelines, and approved by the NIDA Animal Care and Use Committee.

Animals and surgical procedures

Male VGluT2::Cre mice [48], VGAT-ires-Cre (*Slc32a1*$^{tm2(cre)Lowl}$/J) mice or PV::Cre mice (Pvalb$^{tm1(cre)Arbr}$/J mice, in B6;129P2 genetic background and crossed to C57BL/6J mice, from the Jackson Laboratory), breeding at least five generations, 8-10 weeks, were injected into the VTA with AAV5-EF1a-DIO-hChR2(H134R)-eYFP (VGluT2-ChR2-eYFP mice, VGAT-ChR2-eYFP mice or PV-ChR2-eYFP mice). The mice injected with AAV5-EF1a-DIO-eYFP (VGluT2-eYFP mice, VGAT-eYFP mice or PV-eYFP mice) served as controls. VGluT2::Cre mice which were injected with AAV5-EF1a-DIO-hChR2(H134R)-mCherry (VGluT2-ChR2-mCherry mice) were used in confocal and electron microscopy. VGluT2::Cre mice which were injected with AAV-EF1a-DIO-eNpHR3.0-eYFP were used in photoinhibition behavioral experiments. Deeply anesthetized mice were fixed in a stereotaxic apparatus, and 0.3 μl of viral vector (UNC Vector Core Facility) was injected into the VTA (coordinates in mm: AP −3.4, ML ±0, DV −4.3). For anatomical study, male C57BL/6J wild type mice (n = 3) were iontophoretically injected into the nAcc mShell (AP +1.4, ML +0.6, DV −4.7/−4.2) with 1% FG. One week following the FG injection, mice were perfused with 4% paraformaldehyde, and coronal sections of 30 μm for nAcc and 16 μm for VTA were prepared. For dopaminergic terminal lesion studies, 6-hydroxydopamine (0.8 μl, Sigma, 6-OHDA, 3 μg/μl in 0.1% ascorbic acid/0.9% saline) was injected unilaterally into the nAcc mShell, and the vehicle injected mice served as control. For slice

recording, male PV::Cre mice were injected with AAV5-EF1a-DIO-eYFP bilaterally into the nAcc mShell (0.3 μl), and AAV8-hSyn-ChR2-tdTomato into the VTA (0.3 μl). For behavioral testing, we implanted mice with chronic optical fibers directed above the nAcc mShell (AP +1.4, ML ±1.3 at 10°, DV −4.0) at 8 weeks after virus injection. For pharmacological studies in the place conditioning test, mice were implanted with a guide cannula above the nAcc mShell (AP +1.4, ML +0.6, DV −3.5, the microneedle protruded 1 mm to the cannula tip). Mice were allowed at least 10 days recovery before behavioral tests. All mice were housed up to five mice per cage in an animal room at 22°C under a 12 h light/dark cycle (light on at 7 am), with *ad libitum* access to food and water. Behavioral test were performed between 9 am to 6 pm. No multiple behavioral tests were conducted in the same group of animals.

Electron microscopy

Methods were described in previous study [26]. Briefly, vibratome tissue sections were rinsed and incubated with 1% sodium borohydride to inactivate free aldehyde groups, rinsed and then incubated with blocking solution. Sections were then incubated with primary antibodies [mouse anti-mCherry (1:1,000, Clontech Laboraotries, #632543), guinea pig anti-VGluT2 (1:500, Frontier Institute, VGluT2-GPAf240-1) and rabbit anti-PV (1:500, Frontier Institute, PV-Rb-Af750)]. All primary antibodies were diluted with 1% normal goat serum (NGS), 4% BSA in PB supplemented with 0.02% saponin. Incubations were for 24 h at 4°C. Sections were rinsed and incubated overnight at 4°C in the corresponding secondary antibodies. Sections were rinsed in PB, and then in double-distilled water, followed by silver enhancement of the gold particles with the Nanoprobe Silver Kit (2012, Nanoprobes) for 7 min at room temperature. Next, sections were incubated in avidin-biotinylated horseradish peroxidase complex in PB for 2 h at room temperature and washed. Peroxidase activity was detected with 0.025% 3,3′-diaminobenzidine (DAB) and 0.003% H_2O_2 in PB for 5-10 min. Sections were rinsed with PB and fixed with 0.5% osmium tetroxide in PB for 25 min, washed in PB followed by double distilled water and then contrasted in freshly prepared 1% uranyl acetate for 35 min. Sections were dehydrated through a series of graded alcohols and with propylene oxide. Afterwards, they were flat embedded in Durcupan ACM epoxy resin (14040, Electron Microscopy Sciences). Resin-embedded sections were polymerized at 60°C for 2 days. Sections of 65 nm were cut from the outer surface of the tissue with an ultramicrotome UC7 (Leica Microsystems) using a diamond knife (Diatome). The sections were collected on formvar-coated single slot grids and counterstained with Reynolds lead citrate. Sections were examined and photographed using a Tecnai G^2 12 transmission electron microscope (Fei Company) equipped with a digital micrograph 3.4 camera (Gatan).

Ultrastructural analysis of brain tissue

Serial ultrathin sections of the nAcc (bregma 2.76 mm to 0.96 mm) from 4 male VGluT2-ChR2-mCherry mice. Synaptic contacts were classified according to their morphology and immunolabel, and photographed at a magnification of 6,800-13,000×. The morphological criteria used for identification and classification of cellular components or type of synapse observed in these thin sections were as previously described [26]. In the serial sections, a terminal containing greater than 5 immunogold particles were considered as immunopositive terminal. Pictures were adjusted to match contrast and brightness by using Adobe Photoshop

(Adobe Systems Incorporated, Seattle, WA). This experiment was successfully repeated three times. Electron microscopy and confocal analysis quantification was done blindly.

Fluorescence microscopy and 3-D analysis

Methods were described in previous study [26]. Briefly, free floating coronal sections (40 μm) from VGluT2-ChR2-mCherry mice (n = 4) were incubated for 1 h in PB supplemented with 4% BSA and 0.3% Triton X-100. Sections were then incubated with cocktails of primary antibodies: mouse anti-mCherry (1:500) + guinea pig anti-VGluT2 (1:500) + rabbit anti-PV (1:500) overnight at 4°C. After rinsing 3 × 10 min in PB, sections were incubated in a cocktail of the corresponding fluorescence secondary antibodies: Alexa-Fluor-488-anti-guinea pig +Alexa-Fluor-594-anti-mouse + Alexa-Fluor-647-anti-Rb for 2 h at room temperature. After rinsing, sections were mounted on slides. Fluorescent images were collected with an Olympus FV1000 Confocal System (Olympus). Images were taken sequentially with different lasers with 100× oil immersion objectives and Z-axis stacks were collected at 0.2 μm. Imaris microscopy software (Bitplane Inc., South Windsor, CT) was used to analyze Z-stacks of confocal images from 4 VGluT2-ChR2-mCherry mice (64 × 64 × 10 μm for each image, 8 images of nAcc from each mouse) to obtain 3-D quantification of axon terminals expressing mCherry, VGluT2 and cell bodies/dendrites expressing PV. Amira microscopy software (Visualization Sciences Group) was used to analyze Z-stacks of confocal images from 4 VGluT2-ChR2-mCherry mice (64 × 64 × 10 μm for each image, 4 images from each animal) to obtain 3-D reconstruction of putative synapses. This experiment was successfully repeated three times.

Retrograde tract tracing and *in situ* hybridization

Methods were described in previous study [29]. Briefly, midbrain coronal free-floating sections (16 μm) were incubated with rabbit anti-FG (1:1,000, Millipore, AB153) and mouse anti-TH antibody (1:500, Millipore, MAB318), supplemented with RNasin. Sections were rinsed and incubated in biotinylated goat anti-rabbit antibody, fluorescein-conjugated donkey anti-rabbit antibody (1:100; Jackson Immuno Research) and fluorescein-conjugated donkey anti-mouse antibody supplemented with RNasin. Sections were rinsed and transferred to 4% PFA to be visualized by fluorescence with an Olympus BX51 microscope to identify FG and TH-labeled neurons. Sections were rinsed, treated with 0.2 N HCl, rinsed, and then acetylated in 0.25% acetic anhydride in 0.1 M triethanolamine. Sections were rinsed and postfixed with 4% PFA. Before hybridization and after a final rinse with PB, the sections were incubated in hybridization buffer for 2 h at 55°C. Hybridization was performed with buffer containing [^{35}S]- and [^{33}P]-labeled single-stranded antisense rat *vglut2* probes at 10^7 cpm / mL together with the single-stranded rat digoxigenin (DIG)-labeled antisense probe for the two isoforms of rat glutamic acid decarboxylase (*gad65* and *gad67*). Sections were treated with 4 μg/ml RNase A at 37°C for 1 h and washed with 1x saline-sodium citrate, 50% formamide at 55°C for 1 h and with 0.1× saline-sodium citrate at 68°C for 1 h. After the last wash, sections were rinsed with TBS buffer. Afterwards, sections were incubated with an alkaline phosphataseconjugated antibody against DIG for 1-3 hours; alkaline phosphatase reaction was developed with nitroblue tetrazolium and 5-bromo-4-chloro-3-indolyl phosphate yielding a purple reaction product. Sections were then photographed under bright field illumination with an Olympus BX51. Sections were

mounted on coated slides. Slides were dipped in Ilford K.5 nuclear tract emulsion and exposed in the dark at 4°C for 4 weeks before development.

Sections were viewed, analyzed, and photographed with bright-field or epiluminescence microscopy using an Olympus BX51 microscope. Neurons were observed within each traced region at high power (20× objective lenses) and marked electronically. FG-VGluT2, FG-VGluT2-TH, FG-VGluT2-GAD, FG-TH, FG-TH-GAD, FGGAD, FG-VGluT2-TH-GAD, and labeled material was analyzed using epiluminescence to increase the contrast of silver grains, identical to previous reports from our laboratory [18]. For VGluT2 *in situ* hybridization procedures, FG fluorescent cells containing or lacking TH fluorescent signal were photographed before processing for *in situ* hybridization. For radioactive *in situ* hybridization methods (*vglut2* mRNA), a cell was considered to express radioactive transcripts when its soma contained concentric aggregates of silver grains above background level. FG-labeled cells (detected by fluorescence and brown DAB-label) expressing VGluT2 or *gad65/67* mRNA (detected by nonradioactive *in situ* hybridization), and TH (detected by immunofluorescence) were counted separately. FG (brown DAB product), nonradioactive *gad65/67 in situ* hybridization (DIG probe labeled in purple), and radioactive VGluT2 *in situ* hybridization (silver grains) triple-labeled material was analyzed by the following procedure: (1) silver grains corresponding to *vglut2* mRNA expression were focused under epiluminescence microscope, (2) the path of epiluminescence light was blocked without changing the focus, and (3) bright-field light was used to determine whether a brown neuron, expressing FG in focus, contained the aggregates of silver grains seen under epiluminescence. Cells were considered to express DIG-labeled transcripts (*gad65/67* mRNA) when its soma was the same shape as DAB-labeled FG cells. Neurons were counted when the stained cell was at least 5 μm in diameter. Pictures were adjusted to match contrast and brightness by using Adobe Photoshop (Adobe Systems). Cell counting was completed blindly of injection site. Any FG-labeled neuron localized external to the VTA was excluded from analysis.

Combination of in situ hybridization and c-Fos immunolabeling

Methods were described previously [18]. Coronal free-floating sections (16 μm) were incubated for 10 min in PB containing 0.5% Triton X-100, rinsed two times for 5 min each with PB, treated with 0.2N HCl for 10 min, rinsed two times for 5 min each with PB, and then acetylated in 0.25% acetic anhydride in 0.1 M triethanolamine, pH 8.0, for 10 min. Sections were rinsed two times for 5 min each with PB and post fixed with 4% PFA for 10 min. Before hybridization and after a final rinse with PB, the sections were incubated in hybridization buffer (50% formamide, 10% dextran sulfate, 5×Denhardt's solution, 0.62M NaCl, 50 mM DTT, 10 mM EDTA, 20 mM PIPES, pH 6.8, 0.2% SDS, 250 μg/ml salmon sperm DNA, 250 μg/ml tRNA) for 2 h at 55°C. Sections were hybridized for 16 h at 55°C in hybridization buffer containing [^{35}S]- and [^{33}P]-labeled single-stranded antisense of rat dopamine D1 receptor (D1R, nucleotides 228–1,024, GenBank accession number NM-012546.2), or D2 receptor (D2R, nucleotides 1,101–1,681, GenBank accession number M36831) probes at 10^7 cpm/ml. Sections were treated with 4 μg/ml RNase A at 37°C for 1 h, washed with 1×SSC, 50% formamide at 55°C for 1 h, and with 0.1×SSC at 68°C for 1 h. After the last SSC wash, sections were rinsed with PB and incubated for 1 h in PB

supplemented with 4% bovine serum albumin and 0.3% Triton X-100. This was followed by the overnight incubation at 4°C with a rabbit anti-c-Fos antibody (1:1,000, Santa Cruz Biotechnology, SC-52). After being rinsed three times for 10 min each in PB, sections were processed with an ABC kit (Vector Laboratories). The material was incubated for 2 h at room temperature in a 1:200 dilution of the biotinylated secondary antibody, rinsed with PB, and incubated with avidin-biotinylated horseradish peroxidase for 1 h. Sections were rinsed and the peroxidase reaction was then developed with 0.05% 3, 3-diaminobenzidine-4 HCl (DAB) and 0.03% hydrogen peroxide (H_2O_2). The sections were mounted on coated slides. Slides were dipped in Ilford K.5 nuclear tract emulsion (Polysciences; 1:1 dilution in double distilled water) and exposed in the dark at 4°C for 4 weeks before development. Sections were viewed, analyzed, and photographed with bright-field or epiluminescence microscopy using an Olympus BX51 microscope. Neurons were observed within each nAcc shell region at high power (20× objective lenses) and marked electronically.

Behavioral test apparatus

A three-chamber place conditioning apparatus was used for the test, which consisted of two chambers (20 × 18 × 35 cm) with distinct walls patterns and floors, and a connecting chamber (20 × 10 × 35 cm). All animal movements were recorded via camera with a video tracking software.). For both negative-reinforcement task and positive-reinforcement task, sound-attenuated operant chambers were used. Each operant chamber contains a metal grid floor, a house light, and two metal wheels (for negative-reinforcement task) or two retractable levers and a food port (for positive-reinforcement task) installed on a sidewall. An optical encoder and recorded every 90 degrees of rotation for response wheels (Med Associates, St Albans, VT). Chambers were connected to a computer interface with the software (MED-PC for Windows, Med Associates) that controlled all experimental contingencies.

Real-time place conditioning test

Methods were described in previous study [49]. VGluT2::Cre, VGAT-ires-Cre and PV::Cre mice were used in the studies. During the photostimulation pilot study with Latin square design, a group of VGluT2-ChR2-eYFP mice (n = 6) were tested in the conditioning chamber at different light stimulation frequencies (5, 10, 20, 40 Hz) for 10 min. During the real-time place conditioning training and testing, mice were connected to an optical fiber and allowed to access three chambers freely. On habituation and pretest days (15 min session), mice were connected to an optical fiber but the laser was off. Mice showing a side preference (stay less than 150 s in either main chamber) prior to training were excluded. On conditioning days (30 min session), one chamber was assigned as the stimulation chamber (counterbalanced across mice). The animals were given bilateral light stimulation (473 nm, ~5 mW, 10 ms duration at 20 Hz; or 532 nm, ~15 mW, constantly on for photoinhibition conditioning) in nAcc mShell whenever they entered the photostimulation-paired chamber. The stimulation continued until the animal left the photostimulation-paired chamber. On test day (15 min session), mice were allowed to freely explore all chambers without photostimulation. To determine the duration of the acquired aversion, VGluT2-ChR2-eYFP mice were tested for a second time (Test 2 in Supplementary Fig. 2e), 24 hours after the first test day (Test 1).

To test for the participation of glutamate receptors, GABA receptors, and DA receptors in the real-time place conditioning of VGluT2-ChR2-eYFP mice, we applied intra-nAcc microinjections of antagonists against glutamate-receptors (MK801 + CNQX), GABA-receptors (bicuculline + saclofen), D1-receptor (SCH23390), D2-receptor (eticlopride), or a D1 and D2 receptors antagonist mixture. The infusion lasted 1 min, and conditioning test was performed 10 min after infusion. The mice were given optical stimulation on light conditioning day.

Operant negative-reinforcement task

VGluT2-ChR2-eYFP and VGluT2-eYFP mice with chronic optical fibers were trained in an operant negative-reinforcement task. Mice were placed into the operant chambers featured with two wheels. Light stimulation (473 nm, ~5 mW, 10 ms duration at 20 Hz, 0.5 s on/off) was delivered during each session (30 min) daily. For the first six days, the right wheel was designated as the “active wheel”, with each 90° rotation of the wheel producing a 2-s time out from optogenetic activation of the VTA-to-nAcc mShell pathway. Responses on the left wheel were recorded but had no programmed outcome. During the subsequent four reversal training sessions, the left wheel was designated as the “active wheel”.

Operant positive-reinforcement task

VGluT2-ChR2-eYFP and VGluT2-eYFP mice were food restricted to 85% of their free-feeding bodyweight. Mice were placed into operant chambers containing two retractable levers positioned on either side of a food port. Subjects were trained for 1 h per day on an incrementing fixed-ratio (FR) schedule (FR1, FR3, and FR5). Responses on the active lever resulted in the delivery of one 20 mg food pellet and the activation of a 1-s tone and cue light. Sessions concluded at one hour or following the delivery of 50 pellets, whichever occurred first. Once animals had acquired the FR5 task, both levers were presented until mice reached stable responding (defined as 3 continuous days with <20% variability and >250 lever responses). Subsequently, a concurrent variable interval 30-s (VI30) schedule of optical stimulation (1 s of 20 Hz stimulation at 473 nm, ~5 mW, and 10 ms duration) was imposed on the photostimulation-paired lever. Photostimulation was paired with the left lever on sessions 4-5, followed by a no light test on sessions 6, a subsequent reversal of the light pairing (right lever) on sessions 7-8, and a final no light test on session 9.

Learned Helplessness

Methods for the learned helplessness paradigm have been optimized previously [50]. VGluT2-eNpHR-eYFP and VGluT2-eYFP mice with the bilateral optical probe in nAcc mShell were tested in a forced swim protocol to establish a baseline measure for immobility time. Mice were then subjected to a 30 inescapable, un-signaled electric foot shocks (5 s, 0.35 mA; 55 s Inter-Shock interval) over a period of 30 min for 5 daily sessions. Exposure to shock in this manner has been shown previously to produce learned helplessness in mice. Photoinhibition was delivered to eYFP and eNpHR-eYFP mice for a period beginning concomitant with the shock delivery and continuing until 20 s after the termination of each shock. Following the learned helplessness protocol, mice were again tested in the forced swim procedure. The immobile time each animal spent during the test was manually counted offline, with the evaluator being blind to the treatment of the animals. Immobility time was analyzed using a

two-way ANOVA for forced swim test (Pretest vs. Test) and experimental group (eYFP vs. eNpHR).

Slice preparation and optogenetic electrophysiology

Five weeks after virus injection, male PV::Cre mice carrying AAV5-DIO-eYFP in nAcc and AAV8-hSyn-ChR2-tdTomato in VTA (n = 15) were anesthetized with ip injection of chloral hydrate and perfused with ice-cold ACSF, saturated with 95% O_2 and 5% CO_2, and modified to contain (in mM): 92 NMDG, 20 HEPES, 25 glucose, 30 $NaHCO_3$, 1.2 NaH_2PO_4, 2.5 KCl, 5 sodium ascorbate, 3 sodium pyruvate, 2 thiourea, 10 $MgSO_4$, 0.5 $CaCl_2$. Brains were then removed quickly, placed in this same solution on a VT-1200 vibratome (Leica, Nussloch, Germany), and sectioned through the nAcc in coronal slices (200 μm thickness). The slices were placed in a holding chamber filled with the same solution, but held at 32°C. After 15 min, slices were transferred to a holding chamber containing room temperature ACSF modified to contain (in mM): 92 NaCl, 20 HEPES, 25 glucose, 30 $NaHCO_3$, 1.2 NaH_2PO_4, 2.5 KCl, 5 sodium ascorbate, 3 sodium pyruvate, 2 thiourea, 1 $MgSO_4$, 2 $CaCl_2$. For recordings, slices were transferred to a chamber superfused with 32°C ACSF modified to contain (in mM): 125 NaCl, 2.5 KCl, 1.25 NaH_2PO_4, 1 $MgCl_2$, 2.4 $CaCl_2$, 26 $NaHCO_3$ and 11 glucose. Electrodes (4-6MΩ) were backfilled with an internal solution containing (in mM): 140 potassium gluconate, 2 NaCl, 1.5 $MgCl_2$, 10 HEPES, 4 Mg-ATP, 0.3 Na_2-GTP, 10 Naphosphocreatine, 0.1 EGTA and 0.2% biocytin (pH 7.2; 280-290 mOsm). Cells were visualized on an upright microscope using infrared differential interference contrast video microscopy. Whole-cell voltage-clamp recordings were made using a MultiClamp 700B amplifier (2 kHz low-pass Bessel filter and 10 kHz digitization) with pClamp 10.3 software (Molecular Devices, Sunnyvale, CA). PV interneurons and MSNs in the nAcc shell were identified by membrane resistance, resting membrane potential and green fluorescence in the case of PV interneurons. Both neuron populations were voltage clamped at −70 mV, unless otherwise noted. Series resistance (10-30 MΩ) was monitored with a 5 mV hyperpolarizing pulse (50 ms) given every 10 s, and only recordings that remained stable over the period of data collection were used. A 200 μm core optical fiber, coupled to a diode-pumped solid state laser, was positioned just above the slice and aimed at the recorded cell. Optically-evoked EPSCs were obtained every 10 s with pulses of 473 nm wavelength light (8 mW, 5 ms). After evoking EPSC, bicuculline (10 μM) was added in the perfusion ACSF to block GABAa receptors. The peak amplitude of EPSCs was measured with the average of 30 consecutive traces. EPSCs were blocked by bath application of AMPAR antagonist CNQX 10 μM. In some recordings the membrane potential was clamped at −45 mV in order to see GABAergic outward currents.

Fluorescent immunohistochemistry for behavioral testing animals

VGluT2-ChR2-eYFP mice (n = 9) and VGluT2-eYFP mice (n = 8) implanted with nAcc mShell bilateral optical fibers were habituated to the conditioned place preference apparatus for 2 h without light delivery on 3 consecutive days. Following habituation, mice were placed in the apparatus and photostimulation was delivered (473 nm, ~5 mW, 20 Hz, 10 ms duration, 5 s on/off for 15 min). Two hours following the onset of light delivery, mice were perfused and nAcc mShell sections (30 μm) were prepared for fluorescent immunostaining with rabbit anti-Phospho-c-Fos (1:400, #5348, Cell Signaling) and goat anti-PV (1:500,

Frontier institute, PV-Go-Af460), mouse anti-NOS (1:500, Sigma, N2280) or goat anti-ChAT (1:100, Millipore, AB144). The sections were washed and incubated with fluorescent secondary antibody. PV-immunoreactive (IR), NOS-IR or ChAT-IR neurons coexpressing c-Fos-IR neurons were counted based on the confocal images. The neuron quantitation areas are within the nAcc mShell (500 μm × 500 μm). All cell counting was performed blind to the performance of the behavioral animals.

Histological verification

After behavioral testing, all mice were deeply anesthetized and. Coronal sections of nAcc (30 μm) from VGluT2::Cre and VGAT-ires-Cre mice were directly mounted on slides. Free floating coronal VTA sections from VGluT2::Cre and VGAT-ires-Cre mice were washed before incubated in blocking. Sections were then incubated with primary antibodies cocktail: mouse anti-eYFP + rabbit anti-TH antibodies for overnight at 4°C. Sections were rinsed before incubated at room temperature for 2 h in secondary antibodies cocktail. After the slice recording, coronal sections of nAcc from PV::Cre mice were incubated with mouse anti-eYFP + goat anti-PV, and the according secondary antibody, and the biocytin was stained with Cy5. Sections then were rinsed and mounted on slides, and covered with antifade fluorescent mounting medium. Fluorescence images were taken by Olympus VS120 microscope. The nAcc sections from the mice received 6-OHDA lesion were incubated with TH antibody and later DAB staining. After the histological verification, mice with incorrect virus injection, lesion injection, cannula or probe implantation were excluded from data analysis.

Statistics

We performed either a two-side t-test or a one, two or three-way analysis of variance (ANOVA) to analyze all data when applicable. Significant omnibus effects were followed by Newman-Keuls *post hoc* tests (behavioral experiments) or Dunnett's *post hoc* tests (electrophysiology). Statistical analyses were performed with STATISTICA 12 (behavioral experiments), or Graphpad Prism (electrophysiology). Alpha was always set at $P < 0.05$.

Sample size

The target number of samples in each group for behavioral, anatomical, electrophysiological experiments was determined based on numbers reported in published studies. The experimenter performing surgeries, including virus vector injection or probe and cannula implantation, was known to hit the targets used (VTA or nAcc) with a probalility of 0.9. Our target number of animals in each group was 10. We therefore performed about 12 surgeries in each group.

Replication

All sample sizes indicated in figures of behavioral and electrophysiological experiments represent biological replicates. The anatomical and ultrastructural experiments were successfully repeated three times.

Randomization

All randomization was performed by an experimenter. The same stereotaxic apparatus was used for all surgeries. All surgical and behavioral manipulations performed on each animal were determined randomly. For animals used in behavioral experiments, the virus used in each animal and injection site were determined randomly and counterbalanced across groups.

Exclusion criteria

Data were excluded based on predetermined histological and performance criteria established during pilot experiments. Histological criteria included injection sites and optical fiber or guide cannula placement. Only animals with injection sites in the region of interest were included.

Supplementary Material

Refer to Web version on PubMed Central for supplementary material.

Acknowledgements

We thank Drs. O. Kiehn and L. Borgius (Karolinska Institutet) for providing the VGluT2::Cre transgenic mice. We thank Drs. Roy Wise, M. Flavia Barbano and David Root for comments. We thank Bing Liu and Rong Ye for their help in processing brain tissue. The Intramural Research Program of the National Institute on Drug Abuse, US National Institutes of Health (IRP/NIDA/NIH) supported this work.

References

1. Carlezon WA Jr. Thomas MJ. Biological substrates of reward and aversion: a nucleus accumbens activity hypothesis. Neuropharmacology. 2009; 56(Suppl 1):122–132. [PubMed: 18675281]
2. Todtenkopf MS, et al. Brain reward regulated by AMPA receptor subunits in nucleus accumbens shell. J Neurosci. 2006; 26:11665–11669. [PubMed: 17093088]
3. Britt JP, et al. Synaptic and behavioral profile of multiple glutamatergic inputs to the nucleus accumbens. Neuron. 2012; 76:790–803. [PubMed: 23177963]
4. Friedman DP, Aggleton JP, Saunders RC. Comparison of hippocampal, amygdala, and perirhinal projections to the nucleus accumbens: combined anterograde and retrograde tracing study in the Macaque brain. J Comp Neurol. 2002; 450:345–365. [PubMed: 12209848]
5. Grace AA, Floresco SB, Goto Y, Lodge DJ. Regulation of firing of dopaminergic neurons and control of goal-directed behaviors. Trends in neurosciences. 2007; 30:220–227. [PubMed: 17400299]
6. Kelley AE. Memory and addiction: shared neural circuitry and molecular mechanisms. Neuron. 2004; 44:161–179. [PubMed: 15450168]
7. O'Donnell P, Grace AA. Synaptic interactions among excitatory afferents to nucleus accumbens neurons: hippocampal gating of prefrontal cortical input. J Neurosci. 1995; 15:3622–3639. [PubMed: 7751934]
8. Phillips PE, Stuber GD, Heien ML, Wightman RM, Carelli RM. Subsecond dopamine release promotes cocaine seeking. Nature. 2003; 422:614–618. [PubMed: 12687000]
9. Stuber GD, et al. Reward-predictive cues enhance excitatory synaptic strength onto midbrain dopamine neurons. Science. 2008; 321:1690–1692. [PubMed: 18802002]
10. Sesack SR, Carr DB, Omelchenko N, Pinto A. Anatomical substrates for glutamatedopamine interactions: evidence for specificity of connections and extrasynaptic actions. Annals of the New York Academy of Sciences. 2003; 1003:36–52. [PubMed: 14684434]

11. Papp E, et al. Glutamatergic input from specific sources influences the nucleus accumbensventral pallidum information flow. Brain Struct Funct. 2012; 217:37–48. [PubMed: 21643647]
12. Stuber GD, et al. Excitatory transmission from the amygdala to nucleus accumbens facilitates reward seeking. Nature. 2011; 475:377–380. [PubMed: 21716290]
13. Morales M, Root DH. Glutamate neurons within the midbrain dopamine regions. Neuroscience. 2014; 282C:60–68. [PubMed: 24875175]
14. Stuber GD, Hnasko TS, Britt JP, Edwards RH, Bonci A. Dopaminergic terminals in the nucleus accumbens but not the dorsal striatum corelease glutamate. J Neurosci. 2010; 30:8229–8233. [PubMed: 20554874]
15. Tecuapetla F, et al. Glutamatergic signaling by mesolimbic dopamine neurons in the nucleus accumbens. J Neurosci. 2010; 30:7105–7110. [PubMed: 20484653]
16. Van Bockstaele EJ, Pickel VM. GABA-containing neurons in the ventral tegmental area project to the nucleus accumbens in rat brain. Brain Res. 1995; 682:215–221. [PubMed: 7552315]
17. van Zessen R, Phillips JL, Budygin EA, Stuber GD. Activation of VTA GABA neurons disrupts reward consumption. Neuron. 2012; 73:1184–1194. [PubMed: 22445345]
18. Yamaguchi T, Wang HL, Li X, Ng TH, Morales M. Mesocorticolimbic glutamatergic pathway. J Neurosci. 2011; 31:8476–8490. [PubMed: 21653852]
19. Oleson EB, Gentry RN, Chioma VC, Cheer JF. Subsecond dopamine release in the nucleus accumbens predicts conditioned punishment and its successful avoidance. J Neurosci. 2012; 32:14804–14808. [PubMed: 23077064]
20. Pecina S, Berridge KC. Dopamine or opioid stimulation of nucleus accumbens similarly amplify cue-triggered 'wanting' for reward: entire core and medial shell mapped as substrates for PIT enhancement. Eur J Neurosci. 2013; 37:1529–1540. [PubMed: 23495790]
21. Brown MT, et al. Ventral tegmental area GABA projections pause accumbal cholinergic interneurons to enhance associative learning. Nature. 2012; 492:452–456. [PubMed: 23178810]
22. Kawano M, et al. Particular subpopulations of midbrain and hypothalamic dopamine neurons express vesicular glutamate transporter 2 in the rat brain. J Comp Neurol. 2006; 498:581–592. [PubMed: 16917821]
23. Trudeau LE, et al. The multilingual nature of dopamine neurons. Prog Brain Res. 2014; 211:141–164. [PubMed: 24968779]
24. Yamaguchi T, Sheen W, Morales M. Glutamatergic neurons are present in the rat ventral tegmental area. Eur J Neurosci. 2007; 25:106–118. [PubMed: 17241272]
25. Chuhma N, Mingote S, Moore H, Rayport S. Dopamine neurons control striatal cholinergic neurons via regionally heterogeneous dopamine and glutamate signaling. Neuron. 2014; 81:901–912. [PubMed: 24559678]
26. Zhang S, et al. Dopaminergic and glutamatergic microdomains in a subset of rodent mesoaccumbens axons. Nat Neurosci. 2015; 18:386–392. [PubMed: 25664911]
27. Root DH, Mejias-Aponte CA, Qi J, Morales M. Role of glutamatergic projections from ventral tegmental area to lateral habenula in aversive conditioning. J Neurosci. 2014; 34:13906–13910. [PubMed: 25319687]
28. Yamaguchi T, Qi J, Wang HL, Zhang S, Morales M. Glutamatergic and dopaminergic neurons in the mouse ventral tegmental area. Eur J Neurosci. 2015; 41:760–772. [PubMed: 25572002]
29. Root DH, et al. Single rodent mesohabenular axons release glutamate and GABA. Nature neuroscience. 2014; 17:1543–1551. [PubMed: 25242304]
30. Tritsch NX, Ding JB, Sabatini BL. Dopaminergic neurons inhibit striatal output through non-canonical release of GABA. Nature. 2012; 490:262–266. [PubMed: 23034651]
31. Taylor SR, et al. GABAergic and glutamatergic efferents of the mouse ventral tegmental area. J Comp Neurol. 2014; 522:3308–3334. [PubMed: 24715505]
32. Kawaguchi Y, Wilson CJ, Augood SJ, Emson PC. Striatal interneurones: chemical, physiological and morphological characterization. Trends in neurosciences. 1995; 18:527–535. [PubMed: 8638293]
33. Kita H, Kosaka T, Heizmann CW. Parvalbumin-immunoreactive neurons in the rat neostriatum: a light and electron microscopic study. Brain Res. 1990; 536:1–15. [PubMed: 2085740]

34. Li X, Qi J, Yamaguchi T, Wang HL, Morales M. Heterogeneous composition of dopamine neurons of the rat A10 region: molecular evidence for diverse signaling properties. Brain Struct Funct. 2013; 218:1159–1176. [PubMed: 22926514]
35. Parthasarathy HB, Graybiel AM. Cortically driven immediate-early gene expression reflects modular influence of sensorimotor cortex on identified striatal neurons in the squirrel monkey. J Neurosci. 1997; 17:2477–2491. [PubMed: 9065508]
36. Ramanathan S, Hanley JJ, Deniau JM, Bolam JP. Synaptic convergence of motor and somatosensory cortical afferents onto GABAergic interneurons in the rat striatum. J Neurosci. 2002; 22:8158–8169. [PubMed: 12223570]
37. Tepper JM, Wilson CJ, Koos T. Feedforward and feedback inhibition in neostriatal GABAergic spiny neurons. Brain research reviews. 2008; 58:272–281. [PubMed: 18054796]
38. Koos T, Tepper JM. Inhibitory control of neostriatal projection neurons by GABAergic interneurons. Nature neuroscience. 1999; 2:467–472. [PubMed: 10321252]
39. Gittis AH, Nelson AB, Thwin MT, Palop JJ, Kreitzer AC. Distinct roles of GABAergic interneurons in the regulation of striatal output pathways. J Neurosci. 2010; 30:2223–2234. [PubMed: 20147549]
40. Planert H, Szydlowski SN, Hjorth JJ, Grillner S, Silberberg G. Dynamics of synaptic transmission between fast-spiking interneurons and striatal projection neurons of the direct and indirect pathways. J Neurosci. 2010; 30:3499–3507. [PubMed: 20203210]
41. Taverna S, Canciani B, Pennartz CM. Membrane properties and synaptic connectivity of fast-spiking interneurons in rat ventral striatum. Brain Res. 2007; 1152:49–56. [PubMed: 17459351]
42. Koos T, Tecuapetla F, Tepper JM. Glutamatergic signaling by midbrain dopaminergic neurons: recent insights from optogenetic, molecular and behavioral studies. Curr Opin Neurobiol. 2011; 21:393–401. [PubMed: 21632236]
43. Cachope R, et al. Selective activation of cholinergic interneurons enhances accumbal phasic dopamine release: setting the tone for reward processing. Cell Rep. 2012; 2:33–41. [PubMed: 22840394]
44. Threlfell S, et al. Striatal dopamine release is triggered by synchronized activity in cholinergic interneurons. Neuron. 2012; 75:58–64. [PubMed: 22794260]
45. Chang HT, Kita H. Interneurons in the rat striatum: relationships between parvalbumin neurons and cholinergic neurons. Brain Res. 1992; 574:307–311. [PubMed: 1638402]
46. Barker DJ, Root DH, Zhang S, Morales M. Multiplexed neurochemical signaling by neurons of the ventral tegmental area. Journal of chemical neuroanatomy. 2016
47. Wang HL, Qi J, Zhang S, Wang H, Morales M. Rewarding Effects of Optical Stimulation of Ventral Tegmental Area Glutamatergic Neurons. J Neurosci. 2015; 35:15948–15954. [PubMed: 26631475]
48. Borgius L, Restrepo CE, Leao RN, Saleh N, Kiehn O. A transgenic mouse line for molecular genetic analysis of excitatory glutamatergic neurons. Mol Cell Neurosci. 2010; 45:245–257. [PubMed: 20600924]
49. Qi J, et al. A glutamatergic reward input from the dorsal raphe to ventral tegmental area dopamine neurons. Nat Commun. 2014; 5:5390. [PubMed: 25388237]
50. Li B, et al. Synaptic potentiation onto habenula neurons in the learned helplessness model of depression. Nature. 2011; 470:535–539. [PubMed: 21350486]

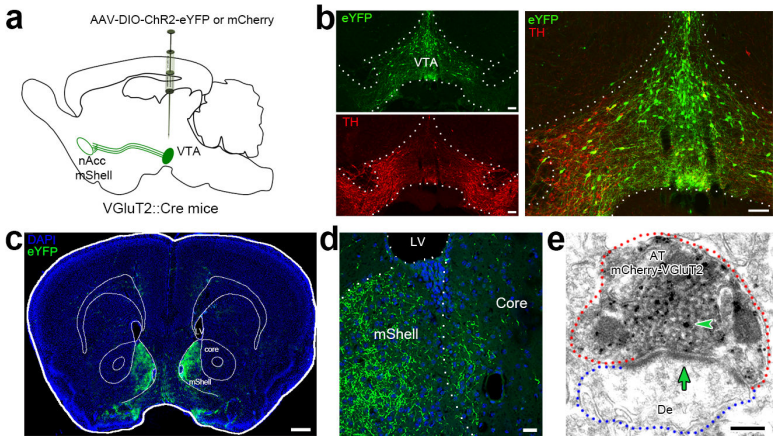

Figure 1. VGluT2 neurons of the VTA make asymmetric synapses on nAcc mShell neurons

(**a**) Diagram of virus injection in VTA of VGluT2::Cre mice. (**b**) VTA neuronal expression of eYFP (green; under *vglut2*-promoter control) within the VTA containing tyrosine hydroxylase (TH; red). (**c** and **d**) Fibers (green) from VTA-VGluT2 neurons are highly concentrated in nAcc mShell. Section counterstained with nuclear dye DAPI (blue). LV, lateral ventricle. (**e**) Axon terminal (AT) containing mCherry-labeling (scattered dark material) and VGluT2-labeling (gold particles, arrowhead) makes an asymmetric synapse (arrow) with a dendrite (De) in nAcc mShell. Bars: (b) 100 μm, (c) 500 μm, (d) 20 μm, and (e) 200 nm.

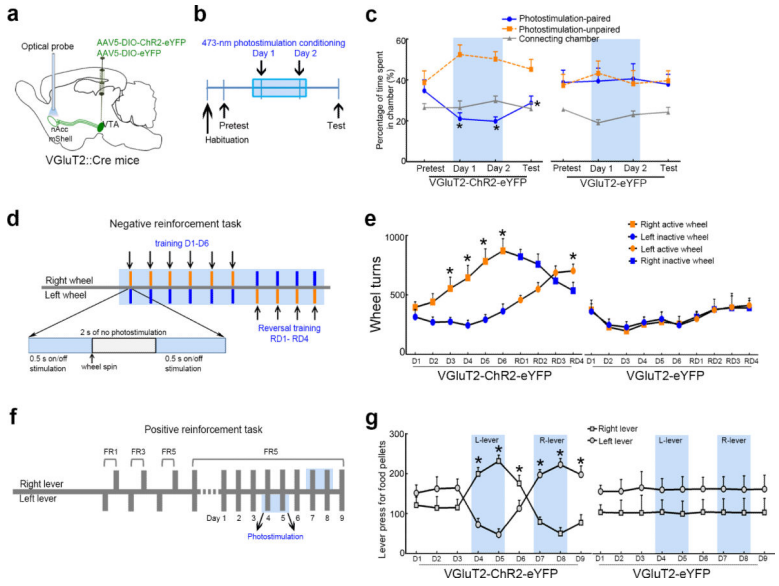

Figure 2. Photostimulation of VTA-VGluT2-inputs to nAcc-mShell results in place aversion and behavioral avoidance in a negative-reinforcement task

(**a**) Diagram of VTA virus injection and nAcc-mShell photostimulation of VTA-VGluT2-inputs. (**b**) Real-time place conditioning procedure timeline. (**c**) During conditioning days, VGluT2-ChR2-eYFP (n =12), but not VGluT2-eYFP (n = 8) mice spent less time in the chamber where nAcc-mShell photostimulation was given. VGluT2-ChR2-eYFP mice showed aversion to the photostimulation-paired chamber on conditioning days and test day ($F_{6,108}$ = 3.085, * P < 0.05, three-way ANOVA with Newman-Keuls *post hoc* test). (**d**) Negative reinforcement task timeline: 6-day negative-reinforcement task training and 4-day reversal training. Wheel turns resulted in 2 s without photostimulation. (**e**) Mice learned a wheel-turning response to avoid photostimulation of VTA-VGluT2-inputs within the nAcc-mShell. VGluT2-ChR2-eYFP (n = 10) but not VGluT2-eYFP (n = 6) mice rotated the “active wheel” significantly more than the “inactive wheel” (* P < 0.05) during the first 6 days ($F_{5,70}$ = 3.287, P = 0.010) and during the 4-day reversal training ($F_{3,42}$ = 6.305, P = 0.001, three-way ANOVA). (**f**) Positive reinforcement task timeline. (**g**) Photostimulation suppresses responding on the photostimulation-paired lever. VGluT2-ChR2-eYFP mice (n = 11) pressed the photostimulation-unpaired lever significantly more than the photostimulation-paired lever. There was a suppression of lever pressing by VGluT2-ChR2-eYFP mice to the left lever during days 4, 5 and 6 ($F_{2,34}$ = 3.7, P = 0.035; three-way ANOVA) and to the right lever during days 7, 8 and 9 ($F_{2,34}$ = 3.38, P = 0.046; three-way ANOVA). * P < 0.05, three-way ANOVA with Newman-Keuls *post hoc* test. Lever pressing by VGluT2-eYFP mice (n = 8) did not change during training sessions when photostimulation was delivered to either the left or right lever. Data are represented as mean + SEM.

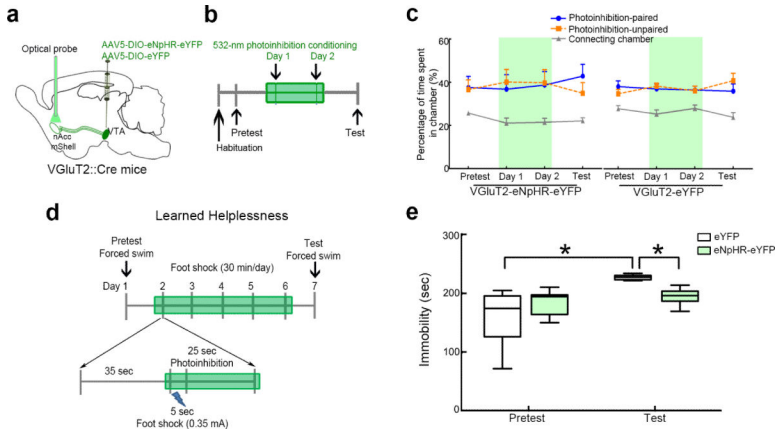

Figure 3. Photoinhibition of nAcc-mShell fibers from VTA-VGluT2 neurons does not change conditioning response, but attenuates foot shock-induced learned helplessness

(**a**) Diagram of virus injection in VTA of VGluT2::Cre mice, and photoinhibition of mesoaccumbens-fibers. (**b**) Real-time place conditioning procedure timeline. VGluT2-eNpHR-eYFP and VGluT2-eYFP mice received nAcc-mShell photoinhibition of mesoaccumbens-fibers during conditioning day 1 and day 2. (**c**) Neither VGluT2-eNpHR-eYFP mice (n =11) nor VGluT2-eYFP mice (n = 9) showed preference or aversion to the chamber where photoinhibition was given (group × day × chamber interaction: $F_{6,108}$ = 1.072, P = 0.384; three-way ANOVA). Relative time spent in each chamber is represented as mean + SEM. Green rectangles indicate photoinhibition available in the photoinhibition-associated chamber. (**d**) Learned helplessness timeline: the forced swim protocol was performed before and after the foot shock training session, in which mice were subjected to 30 unpredicted shocks (5 s, 0.35 mA; 55 s inter-shock interval) over a period of 30 minutes for 5 daily sessions. (**e**) nAcc-mShell photoinhibition of mesoaccumbens-fibers attenuated foot shock-induced learned helplessness. Foot shock significantly increased the immobility in VGluT2-eYFP mice (n = 8) during the forced swim test, but not in VGluT2-eNpHR-eYFP mice (n = 9) (group × day interaction: $F_{1,15}$ = 9.85, P = 0.007; two-way ANOVA, * P < 0.05, Newman-Keuls *post hoc* test).

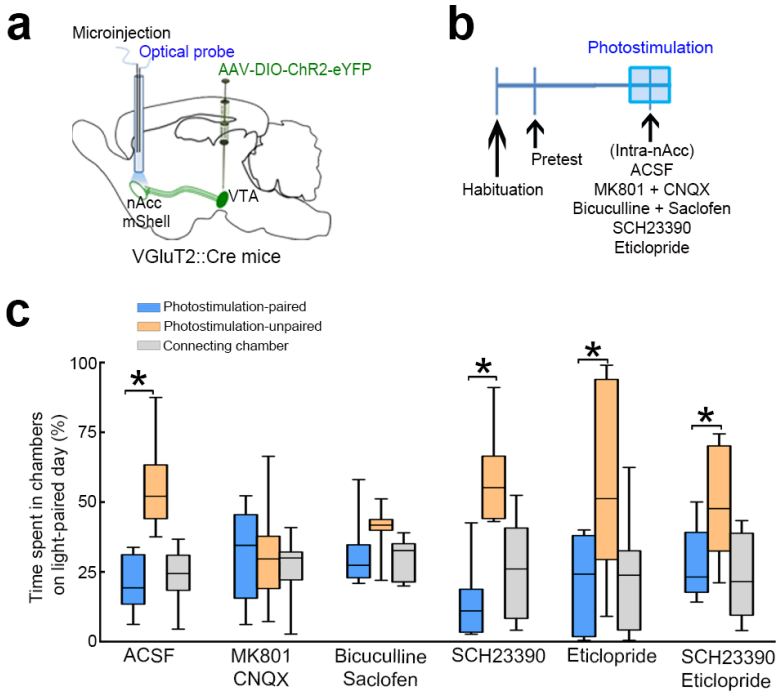

Figure 4. Photostimulation of nAcc mShell fibers from VTA-VGluT2 neurons results in place aversion mediated by glutamate receptors and GABA receptors

(**a**) Diagram of virus injection in VTA, intra-nAcc microinjections of antagonists and nAcc photostimulation of VTAVGluT2 inputs. (**b**) Experimental timeline. VGluT2-ChR2-eYFP mice received intra-nAcc microinjections of antagonists of glutamate-receptors (MK801 + CNQX), GABA-receptors (bicuculline + saclofen), D1-receptor (SCH23390), D2-receptor (eticlopride), or a mix of SCH23390 and eticlopride 10 min prior to photostimulation. (**c**) Effects of intra-nAcc microinjections of antagonists for glutamate-receptors (n = 6), GABA-receptors (n = 7), D1-receptor (n = 7), D2-receptor (n = 7) or a mix of SCH23390 and eticlopride (n = 6) on place aversion induced by nAcc mShell photostimulation. Intra-nAcc ACSF injected mice (n = 11) avoided the photostimulation-paired chamber on training day (*$P < 0.05$). Microinjection of either glutamate-receptor or GABA-receptors antagonists blocked photostimulation-induced place aversion, while antagonists of dopamine-receptors did not (main effect group: $F_{5,38} = 1.35$, $P = 0.266$; group × chamber interaction: $F_{10,76} = 1.7$, $P = 0.096$; two-way ANOVA, *$P < 0.05$, Newman-Keuls *post hoc* test). Data are represented as mean + SEM.

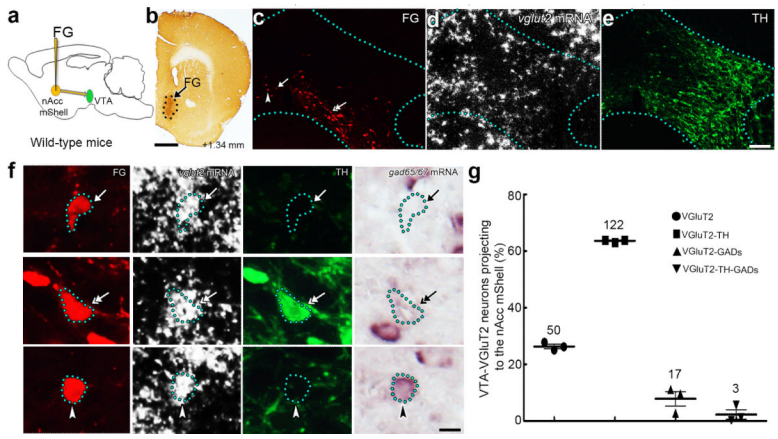

Figure 5. The majority of VTA-VGluT2 neurons projecting to nAcc-mShell lacks *gad65/67* mRNA

(**a**) The retrograde tracer FluoroGold (FG) was delivered into nAcc-mShell. (**b**), FG-immunoreactivity confined at the nAcc-mShell. (**c-f**) VTA detection of FG neurons (red; **c**), *vglut2* mRNA expression (white aggregated grains; **d**) or TH (green; **e**). (**f**). Four phenotypes of FG neurons coexpressing *vglut2* mRNA are seen in VTA; FG-VGluT2-neurons lacking both TH and *gad65/67* mRNA (single arrows); FG-VGluT2-neurons coexpressing TH (double arrows) and FG-VGluT2-neurons coexpressing *gad65/67* mRNA (arrowheads). (**g**) Frequency of the four phenotypes of VTA-VGluT2 neurons innervating the nAcc-mShell (mean + SEM). Among VTA-VGluT2-neurons innervating nAcc-mShell, 26.3 ± 0.8% lacked both TH and *gad65/67* mRNA, 63.6 ± 0.3% coexpressed TH, 7.8 ± 2.5% coexpressed *gad65/67* mRNA, and 2.24 ± 1.6% coexpressed both TH and *gad65/67* mRNA. Neurons were counted from bregma −3.08 mm to −3.88 mm (n = 3 mice, 12-13 sections per mouse). Bars: (b) 250 μm, (e) 100 μm, and (f) 10 μm.

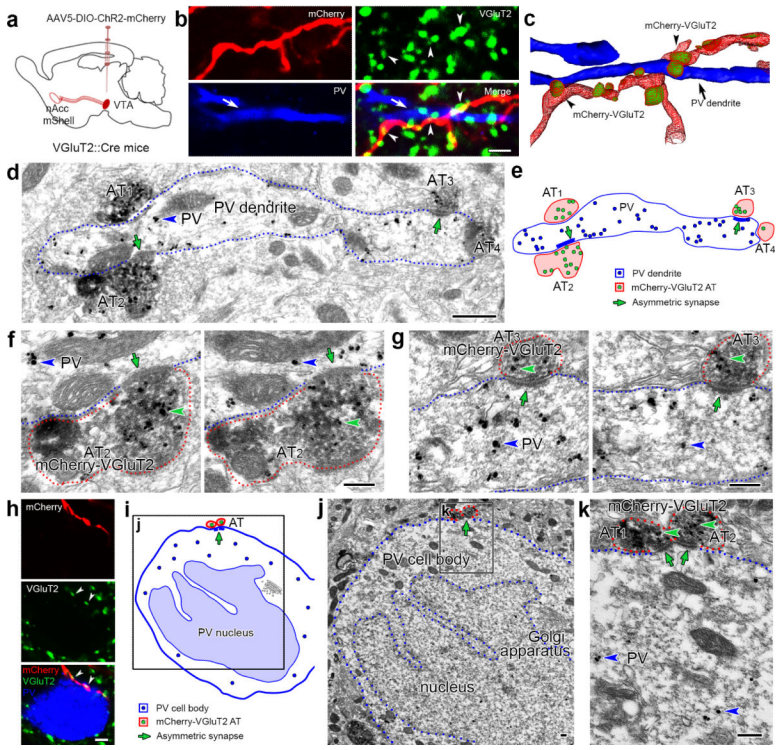

Figure 6. A Single nAcc-mShell PV-interneuron forms asymmetric synapses with several axon terminals from VTA VGluT2-neurons

(**a**) Diagram of fibers from VTA neurons expressing mCherry (under *vglut2*-promoter regulation) innervating the nAcc-mShell (mesoaccumbens axons). (**b-c**) Varicosities from a mesoaccumbens axon coexpressing mCherry (red) and VGluT2 (green) is in contact with a dendrite (arrow) containing PV (blue), contacts are better seen after 3-D reconstruction. (**d-e**) Electron micrograph (d) and corresponding diagram (e) showing detection of PV (gold particles; blue arrowheads) in a dendrite that establishes synaptic contacts with four mesoaccumbens axon terminals (AT_1-AT_4) coexpressing mCherry (scattered dark material) and VGluT2 (gold particles). (**f-g**) Asymmetric synapses (green arrows) between the PV dendrite and both AT_2 (f) and AT_3 (g) in serial sections. (**h**) Varicosities from a mesoaccumbens axon coexpressing mCherry (red) and VGluT2 (green) are in contact (arrowheads) with the cell body of a PV-interneuron (blue). (**i-k**) A cell body expressing PV (gold particles; blue arrowheads) forming an asymmetric synapse (green arrows) with two mesoaccumbens terminals (AT_1 and AT_2) coexpressing mCherry (scattered dark material) and VGluT2 (gold particles; green arrowheads). Bars: (b) 2 μm, (d) 500 nm, (f and g) 200 nm, (h) 2 μm, and (j and k) 200 nm.

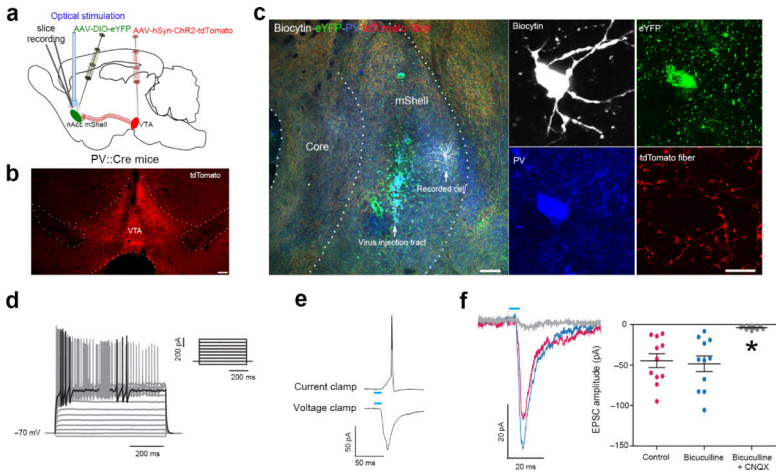

Figure 7. Photostimulation of VTA-fibers evokes EPSCs on nAcc-mShell PV-fast-spiking interneurons

(**a**) Diagram of virus injections in both nAcc and VTA of PV::Cre mice, and photostimulation of mesoaccumbens-fibers in nAcc-mShell during slice recording. (**b**) Virus injection site in VTA. (**c**) nAcc mShell recording of eYFP-fast-spiking-interneuron (green) filled with biocytin (white) showing PV (blue). (**d**) Current clamp responses of a PV-fast-spikinginterneuron to varying current pulses (from −50 pA to +550 pA). Action potentials were initially observed after a current injection of +400 pA (black trace). (**e**) Recording from a single PV-fast-spiking-interneuron demonstrating the response to a single pulse photoactivation of mesoaccumbens-fibers. In current clamp mode, photostimulation elicited an action potential. (**f**) EPSCs recorded at −70 mV in a PV-fast-spiking-interneuron after photostimulation of mesoaccumbens-fibers before (red) or after bath application (10 μM) of bicuculline (blue) or bicuculline + CNQX (gray) (control = −44.78 ± 8.54 pA; bicuculline = −48.54 ± 9.67 pA; bicuculline + CNQX = −4.15 ± 0.69 pA; $F_{2,32}$ =18.86, *P < 0.0001, repeated measures ANOVA, *post hoc* Dunnett's test; n = 11 cells from 7 mice), error bars correspond to SEM. Bars: (b) 100 μm, (c) 100 μm for left panel, and 10 μm for right panel.